Enhanced dielectric standoff and mechanical failure in field-structured composites

James E. Martin, Chris P. Tigges, Robert A. Anderson, and Judy Odinek
Sandia National Laboratories, Albuquerque, New Mexico 87185-1421
(Received 12 May 1998)

We report dielectric breakdown experiments on electric-field-structured composites of high-dielectric-constant $BaTiO_3$ particles in an epoxy resin. These experiments show a significant increase in the dielectric standoff strength perpendicular to the field structuring direction, relative to control samples consisting of randomly dispersed particles. To understand the relation of this observation to microstructure, we apply a simple *resistor-short breakdown model* to three-dimensional composite structures generated from a dynamical simulation. In this breakdown model the composite material is assumed to conduct primarily through particle contacts, so the simulated structures are mapped onto a resistor network where the center of mass of each particle is a node that is connected to neighboring nodes by resistors of fixed resistance that irreversibly short to perfect conductors when the current reaches a threshold value. This model gives relative breakdown voltages that are in good agreement with experimental results. Finally, we consider a primitive model of the mechanical strength of a field-structured composite material, which is a current-driven, *conductor-insulator fuse model*. This model leads to a macroscopic fusing behavior and can be related to mechanical failure of the composite. [S0163-1829(99)14433-3]

I. INTRODUCTION

Particle-filled polymeric resins are widely used to encapsulate electronic components and other devices. These materials generally consist of a thermosetting polymer, such as an epoxy resin, and a particulate phase, such as aluminum oxide, glass microballoons, carbon black, etc. If the dielectric constant of the particulate phase is much larger or smaller than that of the polymeric resin, then it is possible to use applied electric fields to structure the particulate phase to create anisotropic composites that have a number of interesting properties.[1] Composites consisting of chainlike particle, structures can be created by curing the resin in a uniaxial electric field,[2] whereas platelike particle structures can be created by curing in a biaxial field (e.g., a rotating field).[3–5] In particular, when the particulate phase is a material with a large dielectric constant, such as $BaTiO_3$, these field-structured composites can have a permittivity anisotropy of ~ 3, with the permittivity along the structuring field being greater than in the orthogonal direction.[1] The high dielectric constants of these composite materials might be useful for capacitors, but only if the materials also have a high dielectric breakdown field. The experimental investigation of breakdown and the modeling of these results are the main purpose of this paper.

One would *a priori* expect the breakdown field of field-structured composites containing relatively high-permittivity particles to be quite low, due to numerous contacting particles. When a field is applied to such a material, the field enhancement is quite large in the particle gaps whose tangent plane is roughly orthogonal to the applied field, and this can lead to the initiation and propagation of breakdown at relatively low applied fields. There are a large number of such aligned particle gaps when the electric field is applied along the direction of the structuring field, and because the structuring field direction is also the direction of high-permittivity, low-dielectric standoff along this axis would mitigate against the use of such materials in capacitor applications.

The experimental dielectric breakdown measurements we report here are on uniaxial field-structured composites of $BaTiO_3$ particles in an epoxy resin. When the applied field is in the direction of the structuring field, we find only a small, 10% decrease in dielectric breakdown strength compared to unstructured control samples consisting of randomly dispersed particles. Breakdown measurements in the direction orthogonal to the structuring field show a 40–50 % *increase* in dielectric standoff, relative to control samples.

We have found that this anisotropy of the breakdown strength can be understood by applying a voltage-controlled, *resistor-short breakdown model* to three-dimensional field-structured composites generated from a dynamical simulation, the details of which are described at length elsewhere.[2] In this breakdown model the composite material is assumed to conduct primarily through particle contacts, so the simulated structures can be mapped onto a resistor network where the center of mass of each particle is a node that is connected to neighboring nodes by resistors of unit resistance that irreversibly *short* to perfect conductors when the current reaches a threshold value. The strong positive feedback in this model gives roughly one-dimensional (1D) breakdown paths and relative breakdown voltages that are in good agreement with our experimental results.

Finally, we consider a primitive model of the mechanical strength of a field-structured composite material, which is a current-driven *conductor-insulator fuse model*. In this failure model the composite material is again assumed to conduct primarily through particle contacts, so the simulated structures can again be mapped onto a conductor network where the center of mass of each particle is a node that is connected to neighboring nodes by conductors of fixed conductance that irreversibly *blow* to become insulating elements when the current reaches a threshold value. This model gives roughly two-dimensional failure zones and might be relevant

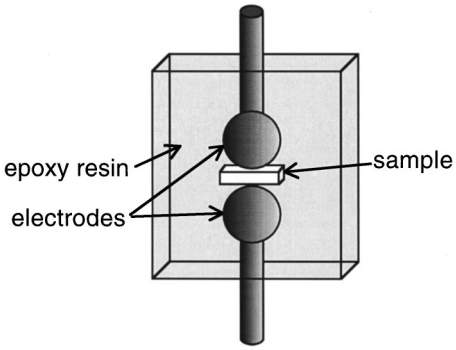

FIG. 1. The test geometry for the dielectric standoff tests.

to the fracture behavior of particle composites and the fusing behavior of carbon-black-filled polymer composites.

In the following we first describe the experimental measurements we performed, then discuss a trivial, one-dimensional model of breakdown, and the methods of modeling breakdown and failure in simulated field-structured composites.

II. EXPERIMENT

A. Sample preparation

The test specimens contained 40 wt% (10.9 vol%) of $BaTiO_3$ powder ($\sim$0.5 μm, Aldrich), in the epoxy resin EPON 828 (a Bisphenol A/Epichlorohydrin based resin) cured with a Jeffamine/Ancamine amine curing agent, in a weight mixture of 75% resin, 25% curing agent. A 1000-Hz, 300-V/mm ac field was capacitively coupled to the sample through Mylar films, and the samples were cured in an oven for 3 h at 70 °C, then post-cured in the absence of the structuring field at 100 °C for 5 h. Both unstructured control samples and structured samples were produced.

Flat wafers were cut from the cured blocks of the loaded epoxy. These were somewhat less than 1 cm square and had nominal thicknesses of 1 mm. The uniaxially structured material was cut in two ways: (1) so that the structuring field was parallel to the wafer thickness direction, i.e., normal to the $\sim$1-cm-square faces; (2) so that the structuring field was perpendicular to the wafer thickness direction, i.e., parallel to the $\sim$1-cm-square face. The former sample we call *z* aligned, since the breakdown field will be applied parallel to the structuring field, which we define as the *z* axis. The latter sample we call *x*-*y* aligned. The control sample was isotropic and thus cut in only one direction.

B. Test geometry

These wafers were loaded into molds, and each wafer was positioned between a pair of polished chrome-steel balls having diameters of 0.5 in. (12.7 mm) which later served as the high-voltage electrodes, Fig. 1. The center of each wafer's faces was aligned with the centerline of the electrodes, and the wafer was held in place by clamping pressure applied through cylindrical conductors which had been attached to the poles of the balls opposite the wafer. An unfilled EPON 828 cured with a Jeffamine/Ancamine amine curing agent was then used to encapsulate the test sample, and bubbles were removed by placing the assembly in an evacuated chamber. The degassed assembly was then cured at 70 °C for 4 h and 100 °C for 18 h, resulting in a transparent block. Visual inspection showed that the clear epoxy filled the tight spaces in the vicinity of the contact between the electrodes and wafer faces. Four samples were prepared for each of the three types of samples: unstructured, *z* aligned and *x*-*y* aligned.

TABLE I. Breakdown voltages and capacitances of $BaTiO_3$-loaded epoxy.

Ordering	Average E_{BD} (kV/mm)	Standard deviation (kV/mm)	Average capacitance (pF)
Unstructured	72	6	2.53
x-*y* aligned	107	18	2.44
z aligned	64	2	2.78

C. Applied voltage

These samples were stressed with high-voltage pulses of a 2-μs rise time and roughly 10-μs duration, at Sandia's High Voltage (HV) pulse facility. The test procedure involved applying an initial pulse with an amplitude near 45 kV, which is below the dielectric strength of the samples, then increasing the amplitude by roughly 20 kV in each successive pulse until breakdown was observed. The time interval between pulses was about 1 min. With this sequence, breakdown happened on the second to fifth pulse. Since breakdown sometimes occurred during the rising portion of the applied-voltage wave form, the breakdown voltage was read from the wave form immediately prior to breakdown. No attempt was made to adjust these values for small (few percent) variations in the thickness of individual samples or for any small indentations from clamping the wafers between the steel spheres.

III. RESULTS

The dielectric strength of barium-titanate-loaded epoxy was found to be strongly affected when the filler particles were microstructurally ordered. Table I lists the average breakdown voltages and the standard deviations we determined. The *z*-aligned samples appear to have a slightly lower dielectric strength than the unstructured samples, but the effect is too small relative to the deviations to be certain of this. However, the *x*-*y*-aligned samples have a breakdown strength roughly 50% larger than the control, and this effect is well outside the deviations of the measurements. The large anisotropy of the breakdown strengths is in good agreement with our primitive breakdown model and is very encouraging in light of possible encapsulated high-voltage device applications.

Average sample capacitances, measured at 100 kHz, are also tabulated in Table I, and the effects of microstructural ordering can be seen there also. Such effects, however, are greatly diminished from the large influence of the encapsulant dielectric surrounding the barium-titanate-loaded wafers, but the trends qualitatively conform to our expectations. By

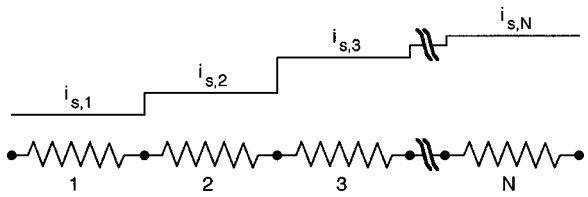

FIG. 2. A one-dimensional model of dielectric breakdown in a voltage controlled system, consisting of resistors of variable short currents connected in series.

comparison, the standoff field of unfilled epoxy exceeds 200 kV/mm.

Post-mortem microscopic inspections of broken down samples revealed fractures radiating from the loaded material into the surrounding clear epoxy. These fractures were presumed to have resulted from high-pressure gas released during a breakdown event, but their location gave no evidence that breakdown paths were located other than very near the electrode centerline, where the electric field was maximal and fairly uniform.

IV. DISCUSSION

A. One-dimensional resistor-short model

To obtain some intuition about some of the issues in dielectric breakdown, we first examine a simple one-dimensional model of breakdown. (We define breakdown as a macroscopic short across the sample.) In this model, disorder is introduced through fluctuations in the characteristics of the network elements (specifically, the short currents), whereas in the field-structured composites disorder is introduced geometrically. Nonetheless, the effect of disorder on the breakdown characteristics is qualitatively similar, as we shall see.

Consider a one-dimensional network of N nonlinear resistors (representing the contact resistance between neighboring particles) each of which will irreversibly short when its critical short current is attained, Fig. 2. Each resistor has a resistance r, so the series resistance of the initial network is $R_t = Nr$. The short current of the resistors is allowed to fluctuate, and the short current of the jth resistor we will call $i_{s,j}$. Because the order in which these resistors are arranged is irrelevant to the breakdown behavior, we will stipulate that $i_{s,j} \leqslant i_{s,j+1}$. We are interested in determining the breakdown behavior of this system, that is, the applied network voltage $V_{s,j}$ required to short each successive resistor.

The voltage required to short the first resistor is $V_{s,1} = I_{s,1} R_t$, where the network current $I_{s,1}$ is trivially equal to the short current $i_{s,1}$ because the network is a simple series of resistors. To short the second resistor the required voltage is $V_{s,2} = I_{s,2} R_t (1 - 1/N)$, where $I_{s,2} = i_{s,2}$, since the network resistance has dropped due to the short. For the kth short, the required voltage is $V_{s,k} = I_{s,k} R_t [1 - (k-1)/N]$ and so forth until the network has completely shorted. By taking the continuum limit, with $x = k/N$, and stipulating that each resistor has a resistance $r = 1/N$, so the series resistance of the initial network is $R_t = 1$, we obtain $V_s(x) = I_s(x)(1-x)$. The breakdown voltage V_b of the network can be found by maximizing $V_s(x)$, i.e., checking for solutions to the equation $dV_s(x)/dx = 0$ on the interval $[0,1]$ and comparing these to $V_s(0)$ and $V_s(1)$.

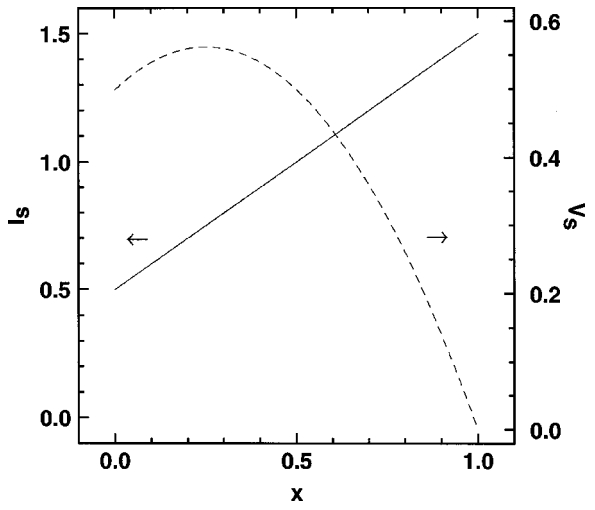

FIG. 3. Short voltage plot for a linear model of the short currents. In this example $a = 1/2$ and $b = 1$. The short voltage reaches a maximum of 9/16 at $x = 1/4$, so there is a substantial regime of progressive shorting that presages catastrophic breakdown.

B. Breakdown modes

It is useful to differentiate between three principal modes of breakdown, and these are best understood by recognizing that breakdown experiments are voltage controlled. *Catastrophic breakdown* occurs when the voltage required to create the first short equals or exceeds the voltage required to create all other shorts. Thus, in a voltage-controlled experiment, ramping up the voltage will lead to a breakdown catastrophy without warning. *Presaged breakdown* occurs when catastrophic breakdown is presaged by a number of shorts at lower voltages. *Progressive breakdown* refers to the case where each successive short requires a higher voltage. Alternatively, the unstable point occurs at $x = 0$ for catastrophic breakdown, at $0 < x < 1$ for presaged breakdown, and at $x = 1$ for progressive breakdown. More complex breakdown scenarios can be devised, but do not seem physically likely.

An example is illustrative. Consider the linear function $I_s(x) = a + bx$. Then $V_s(x)$ has a maximum at $x = (b - a)/2b$. In this case two regimes of behavior are possible: *catastrophic* and *presaged breakdown.*

Catastrophic breakdown occurs when $a \geqslant b$, since then the maximum occurs for $x \leqslant 0$, and on the interval $[0,1]$ the largest breakdown voltage is at $x = 0$. Thus, if the applied voltage is continuously increased to $V_s(0) = I_s(0) = a$, the network will breakdown, with no breakdown events occurring at lower voltage. An extreme and likely example is where all of the short currents for the resistive elements are essentially equal $(b = 0)$.

Presaged breakdown occurs when $b > a \geqslant 0$. In this case the maximum will be on the interval $0 < x \leqslant 1/2$, and upon continuously increasing the voltage, shorts will progressively occur from the voltage $V_s(0) = a$ to the maximum short voltage $V_s[(b-a)/2b] = [(a+b)/2]^2$, at which point the required voltage for successive shorts will decrease, Fig. 3.

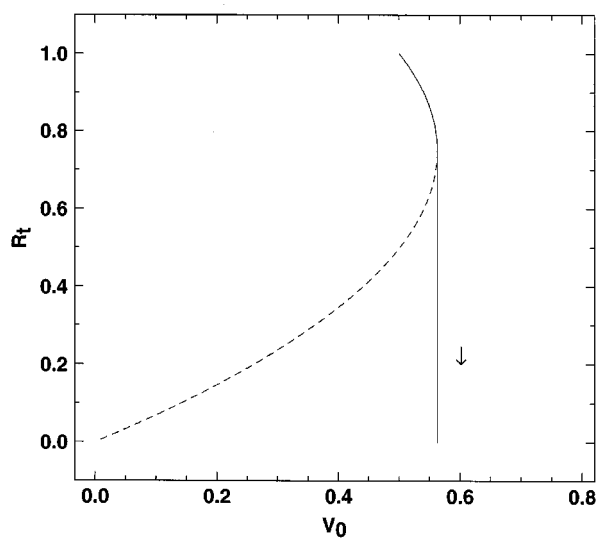

FIG. 4. The one-dimensional series network resistance as a function of applied voltage.

The catastrophic failure that occurs after the maximum voltage is reached is best appreciated in the breakdown plot of Fig. 4, where the network resistance is plotted versus the applied voltage. The resistance starts at 1, until a voltage of 1/2 is reached, where progressive shorts occur until the voltage reaches the breakdown value of $V_b = 9/16$, whereupon the network resistance has decreased to 3/4. At this point breakdown is catastrophic, because successive shorts will occur at lower voltages. In a voltage-controlled experiment, with a continuously increasing voltage, the solid line indicates the network resistance.

Finally, to illustrate progressive breakdown we consider the more complex function $I_s(x) = (a+bx)/(1-x)$. Then the short voltage is $V_s(x) = (a+bx)$, and if $b > 0$, each successive short will occur at increasing voltage, leading to a progressive failure of the network. This type of breakdown behavior seems extremely unlikely in real systems, since a singular distribution of short currents is required to prevent catastrophic failure from occurring at some value of x.

Thus we have seen that in a simple, one-dimensional model some interesting behavior can be observed. In a real system variations in short currents between particles might be due to variations in surface roughness or in the interparticle gaps, or due to low or high dielectric inclusions near the particle surfaces. We shall neglect these effects when considering breakdown in field-structured materials and focus instead on the purely geometrical disorder, although the two types of disorder can certainly be considered simultaneously.

C. Conductivities

Before describing the breakdown model we will first review our method of computing the conductivities of simulated field-structured materials, consisting of conducting particles in an insulating resin. The simulated structures were obtained from a colloidal dynamics algorithm that modeled the structural evolution of 10 000 spherical colloidal particles interacting via induced dipolar interactions with Stokes drag against the suspending liquid and cyclic boundary conditions in all directions.[2] In all cases the structuring field in these simulations was parallel to the z axis and caused preferential ordering along the z axis. To model the anisotropic conductivity of these materials, we make the simple approximation that current conduction is limited by the contact resistance between particles, which we assume is a simple constant (in reality the contact resistance depends logarithmically on the gap and, therefore, on surface roughness, but to some extent the gaps that occur between the spheres in our simulation are affected by finite numerical jitter, so it is probably best to treat the contact resistance as a constant). Thus the particles are mapped onto a simple resistor network, where the particle centers are nodes.

To find the node potentials we used a relaxation method, with local update of the node potential. In this algorithm we made an initial guess of the node potentials, then computed the difference between the actual node potential of the ith particle and the average of the potential of the nodes to which it is connected. The difference ΔV_i was then multiplied by an overcorrection factor of 1.9375 and added to V_i. This overcorrection factor causes the current through the network to converge in a ''critically damped'' fashion that gives 5 to 6 place accuracy in roughly 50 iterations. (Smaller overcorrection values result in slower convergence, and much larger values result in divergences.) The boundary conditions were formulated to ensure that chainlike structures would indeed conduct: particles within 1 radius of the electrodes were fixed at the electrode potential, and all other particle potentials were determined as prescribed. Cyclic boundary conditions were not applied to the electrode faces, but were applied to the other two pairs of faces, to reduce surface effects.

Once Kirchhoff's laws are solved and the network node potentials are found, we compute the current in three ways, all of which should be equal. First, we compute all the current flowing into the particles held at ground potential. Second, we compute the current flowing from the particles held at high potential, which should be equal and opposite. Third, we compute the current flowing through a plane bisecting the sample and parallel to the electrode planes. All of these currents generally agree to ~4–5 places, as indeed they should.

The results of the conductivity calculations are shown in Fig. 5, for materials structured for 75 ms. The field-induced conductivities (at 75 ms) are much larger than those expected for the unstructured material, which shows a classical percolation behavior, being zero until the percolation threshold ϕ_{perc}, then increasing more or less quadratically with $\phi - \phi_{\mathrm{perc}}$. The z-axis conductivity increases almost linearly with ϕ, and the conductivity in the xy plane increases almost linearly with $\phi - \phi_c$, for $\phi > \phi_c$, where ϕ_c is the percolation threshold in the xy plane for samples of 10 000 particles. The anisotropy in the conductivity is strongly dependent on volume fraction and sample size; the data for our system are described by the expression $G_z/G_{xy} \sim (\phi - \phi_c)^{-1.0}$, where $\phi_c = 0.137$. Our studies of percolation in the xy plane indicate that as the system size increases we would expect ϕ_c to decrease, eventually to zero.

The nearly linear increase of the conductivity along the z axis with volume fraction can be rationalized surprisingly well by comparison to a system of chains. A chain of spheres of diameter d that spans a cubical volume L on a side will contain $n = L/d$ spheres. The conductance of this chain will

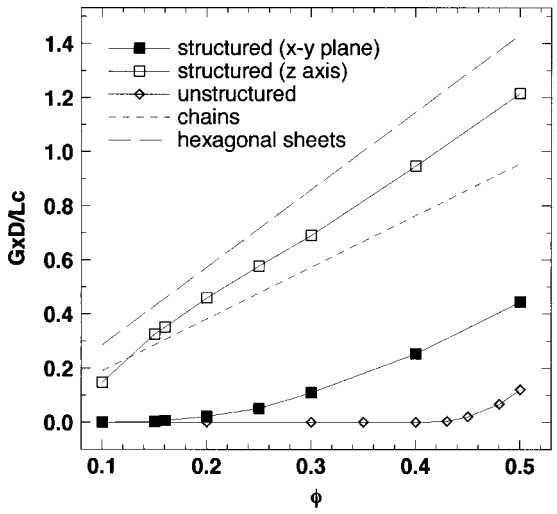

FIG. 5. The computed conductivity of simulated field-structured composites. Here d is the particle diameter, L is the length of the simulation volume on a side, and c^{-1} is the contact resistance.

be $g_{\text{chain}}=c/n$, where c is the inverse contact resistance. The number of such chains in the volume of N spheres will be $m=N/n$, so the conductance of the sample will be $g_z=g_{\text{chain}}m$. The conductivity is then $G_z=g_z/L=c(6/\pi)\phi/d$ or $d\times G_z/c\cong 1.91\phi$. Our computed currents are very close to this, with $d\times G_z/c\cong 2.2\phi$.

The hexagonal sheets and other structures found in our simulated materials give additional current paths. A hexagonal sheet formed of chains aligned along the z axis will have additional current paths that zigzag back and forth between adjacent chains, which are out of registry. Each zigzag path will have half the conductivity of a chain path, and for a sheet there is just one zigzag per chain, so a system of hexagonal sheets will have a conductivity of $d\times G_z/c=(9/\pi)\phi$. Likewise, a system consisting of large body-centered-tetragonal (bct) domains—the ground state for our simulated structures—will have two zigzag paths per chain, so $d\times G_z/c=(12/\pi)\phi$. That the conductivity we observe is greater than the chain limit is due to the presence of these additional current paths.

The conductivity in the x-y plane is much smaller than along the z axis and is not easily explained. The conductivity of a bct lattice in the xy plane is just 3/4 of the conductivity along the z axis, clearly too large to explain the small xy plane conductivities we observe. Even at 50 vol % the x-y conductivity is only about 1/3 of the z axis conductivity. In fact, visualizing the current distributions in the x-y plane shows that these consist of ill-connected domains.

D. Resistor-short breakdown model

In this model of dielectric breakdown the field-structured material is again assumed to conduct primarily through particle contacts and not through the insulating polymeric phase. As the applied field increases, the high fields in the gaps between the high-permittivity particles conduct proportionately more current until they ultimately break down, resulting in an electric short between the particles, which we take to have zero resistance. This short increases the voltage load on nearby contacting particles, driving these to breakdown, etc. The equivalent electrical network is thus defined as for the conduction problem above, but the resistors of resistance c^{-1} now short to perfect conductors when the current passing through a resistor exceeds the short current i_s. Unlike the 1D model described above, where fluctuations in the short currents of the resistors provide the disorder that determines the breakdown behavior, in this model we do not introduce short current fluctuations, but rely only on the geometrical disorder of the material. In a homogeneous material these short current fluctuations are indeed important[6] and lead to fractal, treelike breakdown structures.

The numerical algorithm is straightforward: a unit voltage is applied to the simulation volume and Kirchhoff's laws are solved to find the node potentials. The resistor currents are then computed for this unit applied voltage, and the ''hottest'' resistor, carrying the largest current, is found. We then divide this current into the short current i_s and multiply the applied unit voltage by this factor to determine the applied voltage V_s where this resistor would short. We then short this resistor, recompute the node potentials, find the hottest resistor, short this, etc., until we achieve a perfectly conducting breakdown path that spans the electrodes.

In connection with the numerical method of solving this model, one technical note is worthy of mention: the fast relaxation method we use to solve Kirchhoff's laws converges when the potential of each node is equal to the conductance-weighted average of the potentials of the neighboring particles. Thus the shorted elements completely dominate the weightings. If two nodes are connected by a short, they solely determine each others potential, and this potential will tend to float in a meaningless fashion relative to the other neighboring nodes, with our numerical relaxation method. Our solution to this numerical problem is to group nodes connected by shorts into ''clusters.'' Each cluster will be an equipotential and will be connected via nonshorted resistors to all the neighbors of all the cluster member nodes. Thus a cluster is simply a high functionality node. Each successive short simply requires a new mapping of the nodes onto a network of fixed resistance resistors.

E. Breakdown paths

To obtain reasonable estimates of the average breakdown voltage in field-structured composites, we first ran a total of four simulations of $N=10\,000$ particles out to 75 ms at concentrations of 20, 30, 40, and 50 vol % particles. This gives us a total of 8 breakdown simulations in the x-y plane and 4 along the z axis, for each concentration. It is well known that breakdown phenomena tend to be intrinsically noisy, presumably because a defect of some kind can trigger breakdown. We found that even when the only source of noise in the system is the geometrical disorder we generate in our simulations there are still large sample-to-sample variations in the breakdown voltage. Reasonable statistics are obtained by averaging over 4 simulations.

Some examples of the breakdown behavior we observe are shown in the figures for a sample at 40 vol %. In Fig. 6 the field is applied along the y axis, and the composite material is shown viewed along the z axis, both in a real space image and in a current-voltage representation, before breakdown. In the latter image, the particles in contact with the

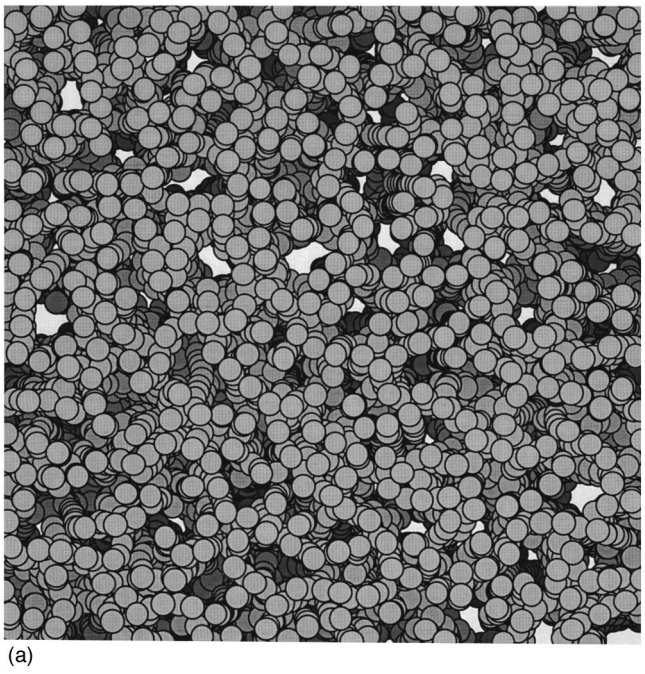

FIG. 6. Dielectric breakdown along the y axis at $\phi = 40$ vol %, viewed along the z axis. (a) The structure of a simulated field-structured material after a 75-ms exposure to a structuring field. (b) (Color) The particle voltage and currents are visualized: Particles in contact with the ground electrode are at the bottom, particles in contact with the high potential electrode are on top, and the interior particles are sized in proportion to their currents and colored according to their potential.

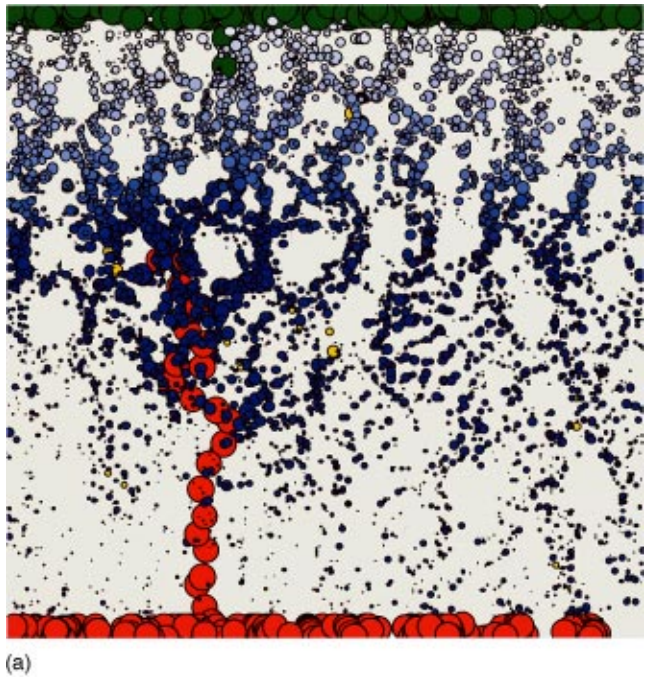

FIG. 7. Dielectric breakdown along the y axis at $\phi = 40$ vol %, viewed along the z axis. Particles connected by shorts are shown full size, and the other particles are sized according to their currents. (a) (Color) The evolving breakdown path is shown after 35 shorts. (b) The evolving breakdown path is shown just before the final, 49th short. The current screening is readily apparent.

electrodes are shown full size and in a unique color. The gradation in color of the floating potential particles indicates their potential, whereas their size indicates the current passing through them. Breakdown initially occurs via the formation of isolated shorts throughout the system, until a critical short occurs. We found that the critical short may occur at either electrode or within the floating potential particles. At least once a breakdown path emanating from the high-potential electrode was met by a path from the ground electrode. An interesting aspect of Fig. 7 is the strong current screening behind the breakdown path. This occurs because the breakdown path is a projecting equipotential. Large currents emanate from its tip, making this the most likely place for further breakdown, and this positive feedback results in a rather low-dimensionality structure being formed. Breakdown along the y axis was achieved after 49 shorts, which is

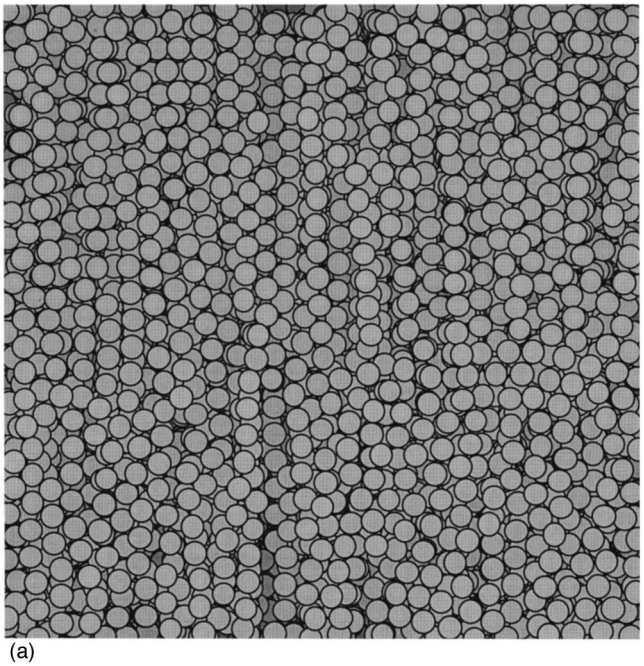

FIG. 8. Dielectric breakdown along the z axis at $\phi = 40$ vol %, viewed along the y axis. (a) The structure of the same simulated field-structured material shown in Fig. 6. (b) (Color) The particle voltages and currents are visualized, as in Fig. 6.

quite close to the average for breakdown in the x-y plane at this particle concentration. The simulation volume is 23.6 particle diameters across, so more than twice as many shorts occurred as were required merely to make a strictly linear breakdown path.

The breakdown behavior along the z axis, Figs. 8 and 9, is quite different. First, the breakdown path is much more linear, requiring only 26 shorts in the case given and an average of 28 at $\phi = 40$ vol %. Second, the current screening effect is not nearly as pronounced. These two observations might seem at odds, but here the low dimensionality of the breakdown path is assured by the low dimensionality of the chainlike structures along the z axis. Finally, in Fig. 10 a comparison is given between the breakdown behaviors along the y and z axes. Along the y axis a number of disconnected shorts are obvious and the breakdown path is much more tortuous.

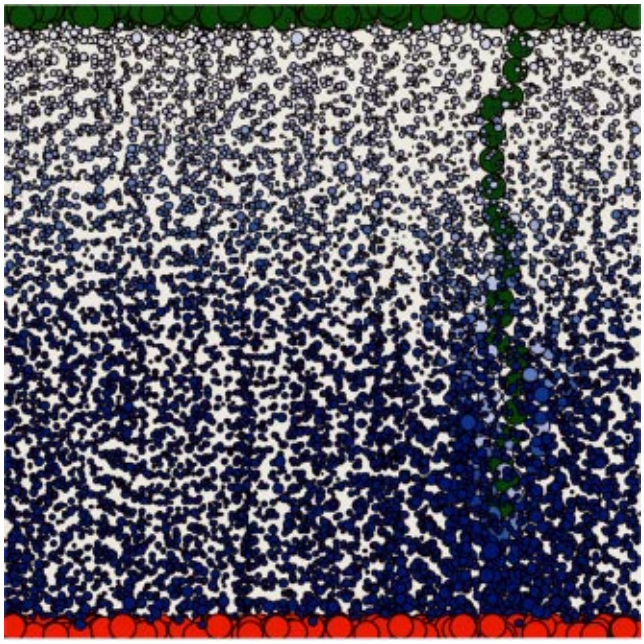

FIG. 9. (Color) Dielectric breakdown along the z axis at $\phi = 40$ vol %, viewed along the y axis. The evolving breakdown path is shown after 20 shorts.

F. Breakdown behavior

The breakdown behavior along the y and z axes is shown in Fig. 11, as a plot of the computed resistance against the short voltage. Note the qualitative similarity of this plot to the behavior predicted for the one-dimensional model, Fig. 4, under conditions of presaged breakdown. Along both the y and z axes, the resistances start out high and monotonically decrease with each successive short. Along the y axis there are quite a number of shorts that presage the catastrophic breakdown that occurs at an applied voltage of $cV_s/i_s = 23.7$. In fact, before catastrophic breakdown, the shorts will actually occur in several bursts of a few shorts each. Along the z axis the drop in sample resistance does not appear so striking, simply because the sample resistance starts out low in this case due to the many conducting paths. Relatively few shorts presage breakdown in this case, and the breakdown voltage is only $cV_s/i_s = 13.3$.

The total number of shorts at breakdown and the number of shorts that presage catastrophic breakdown are shown in Figs. 12 and 13. The number of shorts required in the x-y plane is $\sim$ twice that required along the z axis, due to both the large number of shorts that presage catastrophic breakdown in the former case and because of the increased tortuosity of the breakdown path. The number of shorts that presage breakdown is large in the x-y plane and fluctuates a great deal. Along the z axis the number of presaging shorts is much smaller and becomes insignificant at higher concentrations, where essentially catastrophic breakdown occurs.

Finally, the dielectric breakdown strength as a function of particle volume fraction is shown in Fig. 14. The enhance-

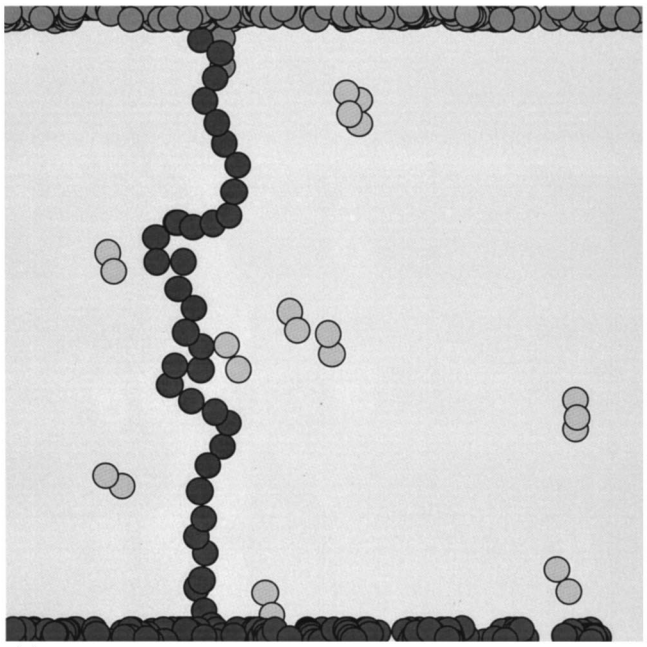

FIG. 10. Comparison of simulated (a) *y*-axis and (b) *z*-axis breakdown paths at 40 vol %.

ment of the breakdown strength in the *x*-*y* plane relative to the *z* axis is clear and is in good agreement with the 50% enhancement observed experimentally. It is somewhat surprising that the enhancement effect even applies to very large particle concentrations. This result, coupled with our experimental findings, argues for the structuring of the particle phase in situations where breakdown might occur, such as devices containing encapsulated high-voltage power supplies.

G. One-dimensional conductor-insulator fuse model

We now consider a current-controlled network of conductors, each of which is a fuse that will blow at a threshold voltage to an insulating element. Physically, this fuse blowing might correspond to the effect of thermal expansion of an insulating polymeric resin between conducting particles, thus increasing the contact resistance, or it might correspond to fracture of a mechanical network, as discussed below.

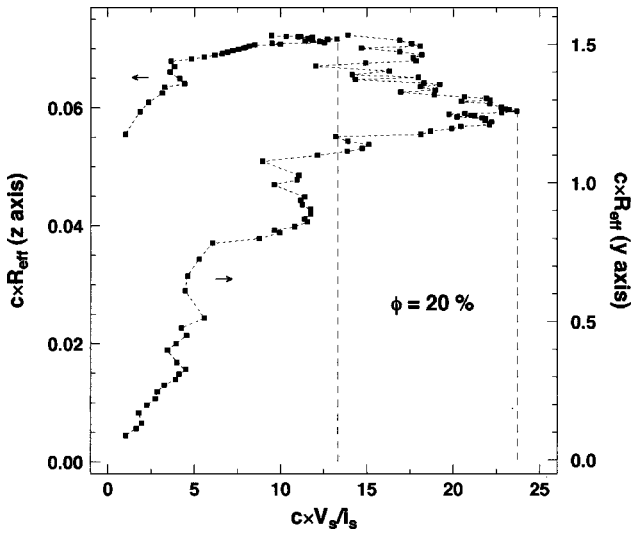

FIG. 11. The sample resistance is plotted against the short voltage. The vertical dashed lines indicate the breakdown voltage. Note that to follow the progression of breakdown one must start at the top of these curves.

In Fig. 15 is a schematic of a one-dimensional network of N parallel nonlinear conductors (representing the contact resistance between neighboring particles) each of which will irreversibly blow to an insulator when its critical fuse voltage is attained. Each conductor has a conductance g, so the parallel conductance of the initial network is $G_t = Ng$. The fuse blow voltage of the conductors is allowed to fluctuate, and the fuse blow voltage of the jth resistor we will call $V_{f,j}$.

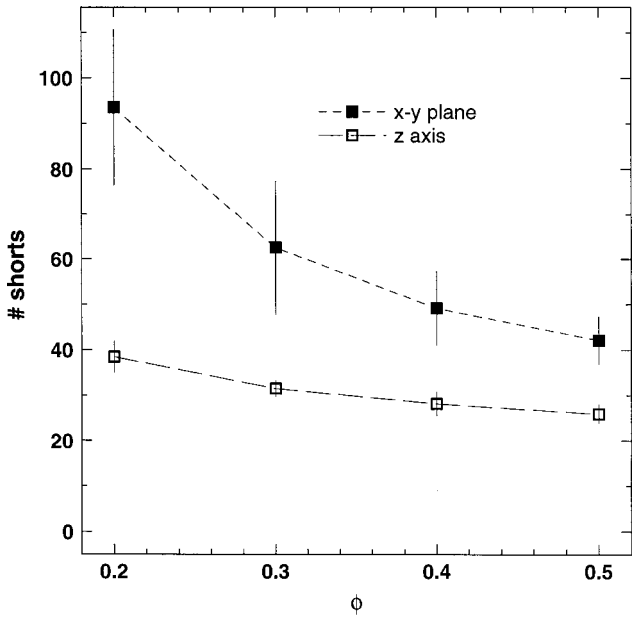

FIG. 12. The total number of shorts after breakdown for the simulated structures. The number of shorts required in the *x*-*y* plane is ~ twice that required along the *z* axis.

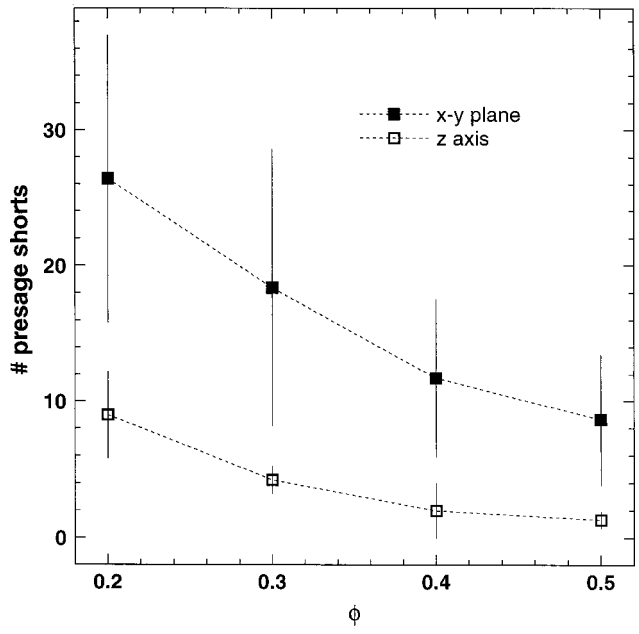

FIG. 13. The number of shorts that presage breakdown is large in the *x-y* plane and also has large fluctuations. Along the *z* axis the number of presaging shorts is much smaller, and becomes insignificant at higher concentrations, where essentially catastrophic breakdown occurs.

Because the order in which these fuse conductors are arranged is irrelevant to the failure behavior, we will stipulate that $V_{f,j} \leqslant V_{f,j+1}$. We are interested in determining the failure behavior of this system—the applied current $I_{f,j}$ required to blow each successive conductor.

The network current required to blow the first conductor is $I_{f,1}=V_{f,1}G_t$. To blow the second conductor the required current is $I_{f,2}=V_{f,2}G_t(1-1/N)$, since the network conductance has dropped due to the blown fuse. For the kth fuse, the required network current is $I_{f,k}=V_{f,k}G_t[1-(k-1)/N]$

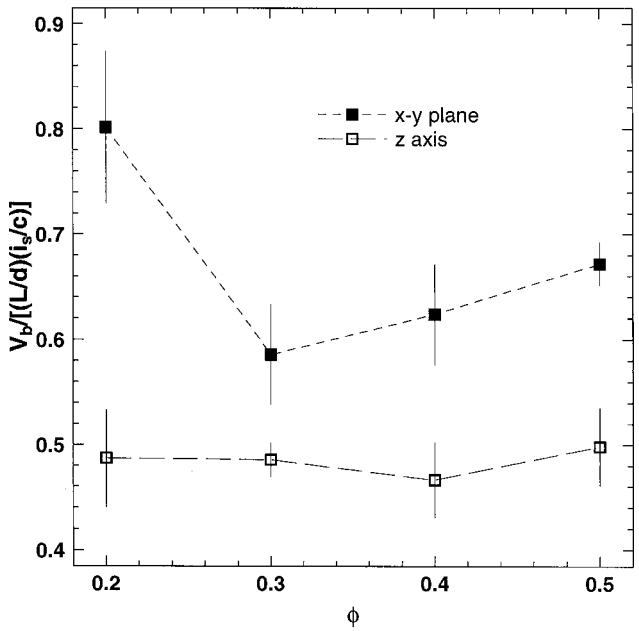

FIG. 14. The dielectric breakdown strength as a function of particle volume fraction for the simulated structures.

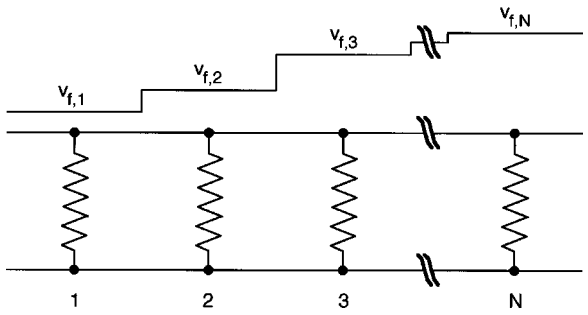

FIG. 15. A one-dimensional model of failure in a current controlled system, consisting of conductors of variable short voltages connected in parallel.

and so forth until the network has completely blown. By taking the continuum limit, with $x=k/N$, and stipulating that each conductor has a conductance $g=1/N$, so the parallel conductance of the initial network is $G_t=1$, we obtain $I_s(x)=V_s(x)(1-x)$. The breakdown current I_b of the network can be found by maximizing $I_s(x)$, i.e., checking for solutions to the equation $dI_s(x)/dx=0$ on the interval [0,1] and comparing these to $I_s(0)$ and $I_s(1)$.

At this point the perspicacious reader will note that these last two paragraphs were synthesized from the previous two paragraphs describing the ''one-dimensional resistor-short model'' by substituting the variable g for r, G for R, I for V, and V for I. Since these two one-dimensional models are isomorphic, all of the results obtained for the previous 1D model apply here as well, with the appropriate redefinition of variables, and we need not reiterate those results. The essential point is that in a parallel network of conductors strong positive feedback occurs when the device is current driven. Before proceeding to the application of this model to simulated composite structures, we first describe the connection of this model to fracture.

H. Analogies between electrical and mechanical networks

For the one-dimensional series and parallel electrical network models we have described, there are obvious connections to the failure of one-dimensional series and parallel spring networks. (The connection of the conductivity of a resistor network to the elasticity of a spring network was first pointed out by Last and Thouless.[7]) Consider the series resistor-short case first. Kirchhoff's law for a series network is $\Sigma_j g_{ij}(v_i-v_j)=0$, where the sum extends over the (two) neighbors of the ith node and g is the conductivity of the resistor connecting the ith and jth nodes, and v is the node voltage. The boundary condition for this network is that the voltage drop is V_0 or $\Sigma_{i=1}^{N-1}(v_i-v_{i+1})=V_0$. For a 1D spring model a force balance gives $\Sigma_j k_{ij}(x_i-x_j)=0$, where k is a spring constant and x is the node position. A fixed deformation boundary condition satisfies $\Sigma_{i=1}^{N-1}(x_i-x_{i+1})=X_0$, where X_0 is the applied deformation. Thus the mapping of electrical resistor networks to mechanical spring networks is straightforward: voltage is like position: current density is like stress. Controlled voltage means controlled deformation, and controlled current density means controlled stress. The network conductivity is analogous to the network modulus.

The breakdown failure mechanism for the electrical network is that the resistor whose current exceeds its threshold value shorts, so $g_{ij}\rightarrow\infty$ and $v_{ij}\rightarrow 0$. In the spring network this corresponds to a strange and probably unphysical instability where a spring whose stress exceeds its threshold value will undergo a deformation collapse, so that $k_{ij}\rightarrow\infty$ and $x_{ij}\rightarrow 0$. Because the mechanical system is at fixed deformation, the contraction of each bond will increase the stress on each remaining bond.

This mechanical analogy of the resistor-short breakdown model does not seem physical to us, but the conductor-insulator fuse model is analogous to a primitive model of network failure: the controlled current density is like applying a controlled stress, and each fuse event causes $g_{ij}\rightarrow 0$, analogous to $k_{ij}\rightarrow 0$, i.e., bond fracture. The current density where the macroscopic electrical network fuses is like the stress where the spring network fractures.

For three-dimensional networks the analogy breaks down somewhat, due to the vector nature of forces. For a 3D resistor network, it is still true that the node potentials satisfy $\Sigma_j g_{ij}(v_i-v_j)=0$: however, for a 3D spring network the node positions must satisfy the vector relation $\Sigma_j k_{ij}(\mathbf{r}_i-\mathbf{r}_j)=0$. Thus the analogy is no longer exact, but is still instructive. In particular, this analogy could be useful in modeling failure in the case where the adhesive strength of the polymeric resin between contacting particles greatly exceeds the cohesive strength of the resin—a reasonable assumption in many cases—and where the stress intensity factor of the stress tip is low, such as might be the case if the resin is above the glassy transition temperature.

I. Conductor-insulator fuse model

In this current-driven model, the structure is mapped onto an equivalent circuit just as described previously, but now the fuse conductors, of conductance c, blow to insulators when the voltage across a conductor exceeds the threshold v_f. The implementation of this algorithm is similar, but simpler technically, than that described for the resistor-short model; a unit voltage is applied to the simulation volume and Kirchhoff's laws are solved to find the node potentials. The voltage drops across the conductors are then computed for this unit voltage, and the ''hottest'' conductor, with the largest voltage drop, is found. We then compute and record the minimum applied voltage required to blow this conductor, and then we open this conductor before recomputing the node potentials. This process is continued until we achieve failure, in this case a platelike instability of blown fuses that prevent current flow.

J. Failure instabilities

To obtain reasonable estimates of the average failure current in field-structured composites, we used the same simulation volumes as in the resistor-short study; four simulations of $N=10\,000$ particles run out to 75 ms at each of the concentrations of 20, 30, 40, and 50 vol % particles. This again gives us a total of 8 failure simulations in the x-y plane and 4 along the z axis, for each concentration.

Unlike the resistor-short breakdown model, which gives breakdown instabilities that are essentially one dimensional, the conductor-insulator fuse model gives roughly two-dimensional instabilities, since a blown fuse tends to cause current to be redirected to nearby parallel current paths. Some examples of the failure behavior we observe are shown in the figures for a sample at 50 vol %. In Fig. 16 the composite material is shown viewed along the z axis (ordering axis), both in a real space image and in a current-voltage representation, before failure. In the latter image, the particles at the electrodes are shown full size and in a unique gray scale. Again, the gradation in gray scale of the interior

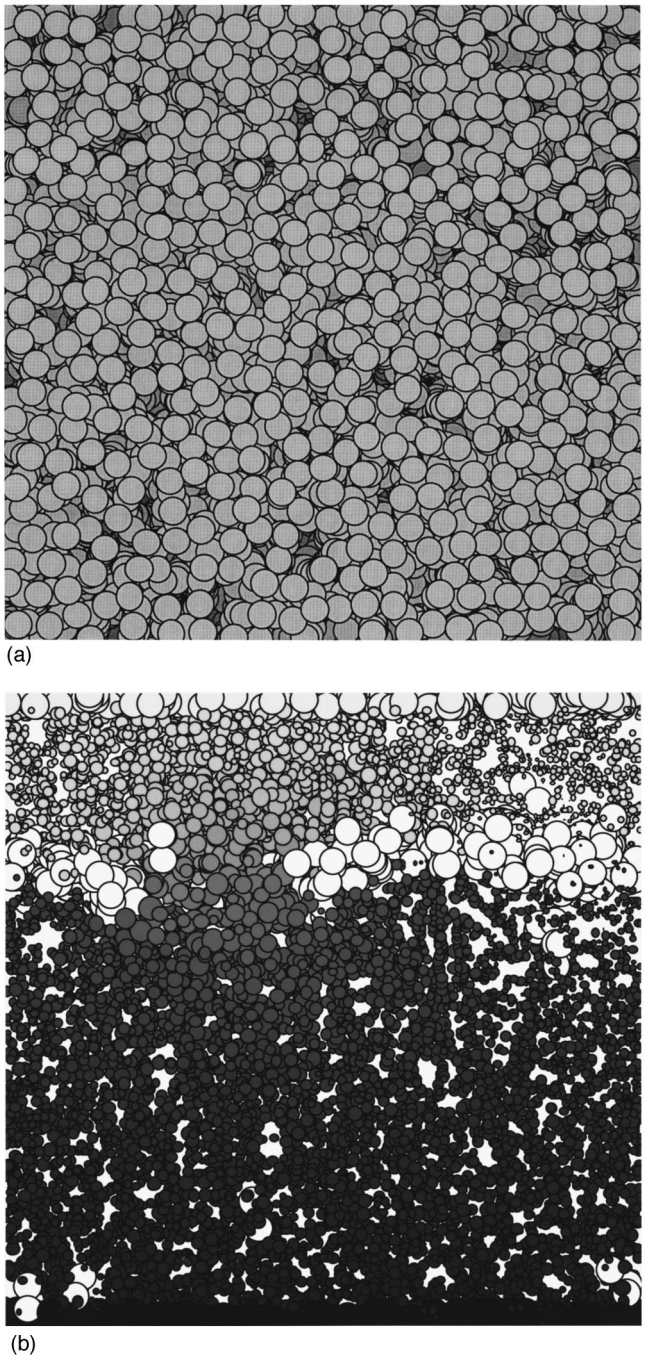

FIG. 16. z-axis views of a simulated field-structured material. Image (a) shows the structure, and image (b) shows the progression of failure with the field applied along the y axis, with particle size indicating current, except for electrode-contacting particles and those that are connected, so to speak, by fused conductors, which are full sized. Image (b) is after 250 fuse breaks.

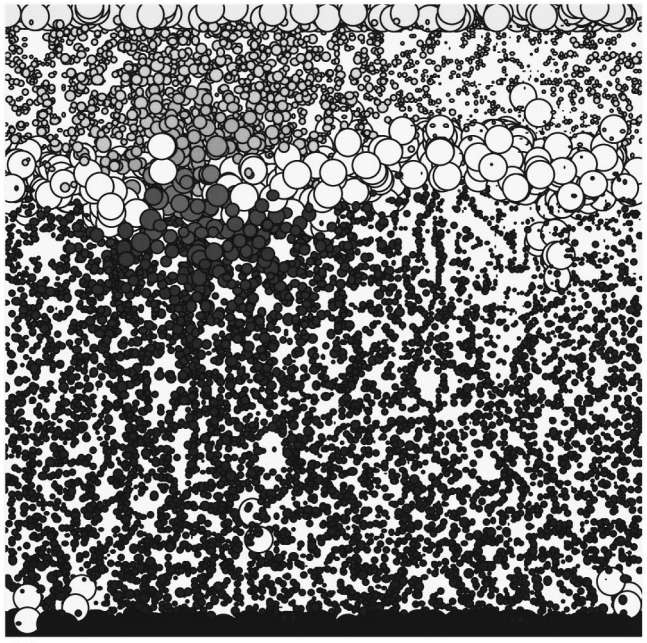

(a)

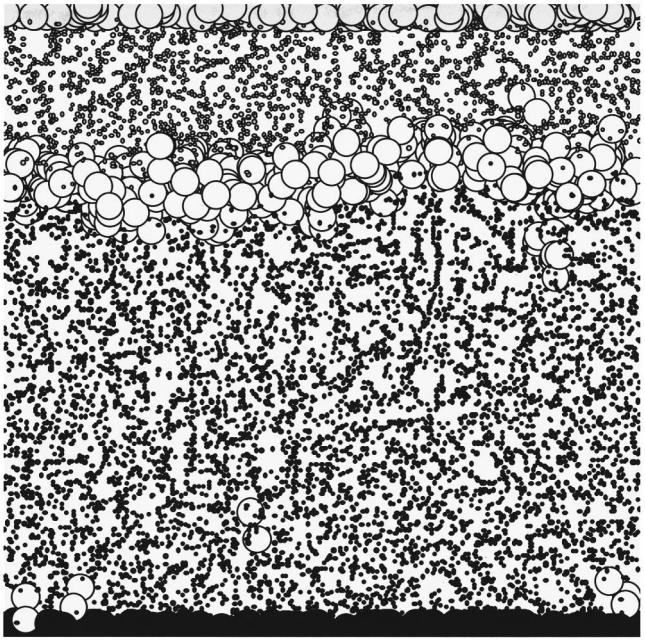

(b)

FIG. 17. *z*-axis views of the simulated field structured material shown in Fig. 16. Image (a) is after 300 breaks and shows strong current screening, whereas image (b) is after the final 319 fuse events (here the interior particles have a fixed small size that merely indicates their position, not their currents, which are zero) and clearly shows the roughly planar failure zone. At lower particle concentrations the failure zone becomes progressively rougher.

particles indicates their potential, whereas their size indicates the current passing through them. Failure initially occurs via the formation of isolated blows throughout the system, until a critical blow occurs at a maximum applied current. An interesting aspect of Fig. 17, which shows the evolution of blows closer to and at failure, is the strong current screening caused by the evolution of the sheetlike failure.

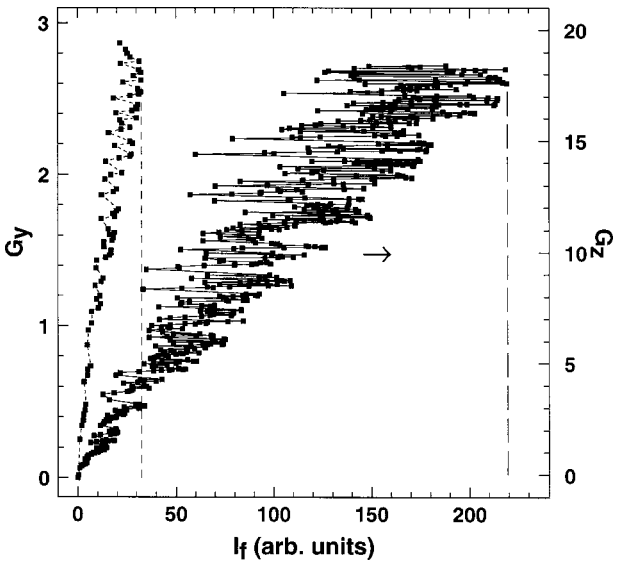

FIG. 18. The conductance of a 30 vol % simulated field-structured composite is plotted against the fusing current. The vertical bars indicate the conductance where macroscopic failure occurs, which is much larger along the *z* axis. Along both axes the macroscopic fusing is presaged by a small number of blows. The plot is very similar to the resistor-short results in Fig. 11, except the effect is much larger.

K. Failure behavior

The simulated failure behavior along the *y* and *z* axes is shown in Fig. 18, for a 30 vol % sample, as a plot of the computed conductance against the fuse blow current. This plot bears a qualitative similarity to the behavior of the resistor-short breakdown model, Fig. 11, but now the failure anisotropy is much larger. Along both axes there are a number of blows that presage the catastrophic failure indicated by the dashed lines. The positive feedback is strong beyond the failure current, but the system still exhibits a lot of noise.

The total number of blows at failure is shown in Fig. 19. The number of fuse blows required along the *z* axis is much larger than that required in the *x*-*y* plane, due to the much larger number of current-carrying paths in the *z* direction. The large number of current paths also results in more conductance, so the number of blows at failure tends to be proportional to the conductance of the sample. In a mechanical system this would be analogous to the fracture energy increasing with the elastic modulus.

Finally, the simulated failure current as a function of particle volume fraction is shown in Fig. 20. The enhancement of the failure current along the *z* axis relative to the *x*-*y* plane is quite large, unlike the breakdown model, where the *x*-*y* plane shows a slightly greater breakdown strength. In Fig. 21 we show that the number of blows at failure is proportional to the breakdown current. Data are included for both the *x*-*y* plane and the *z* axis over the full concentration range we investigated.

L. Application to composite materials

Composite materials made of conducting carbon black particles in poly(ethylene) are known to exhibit a positive

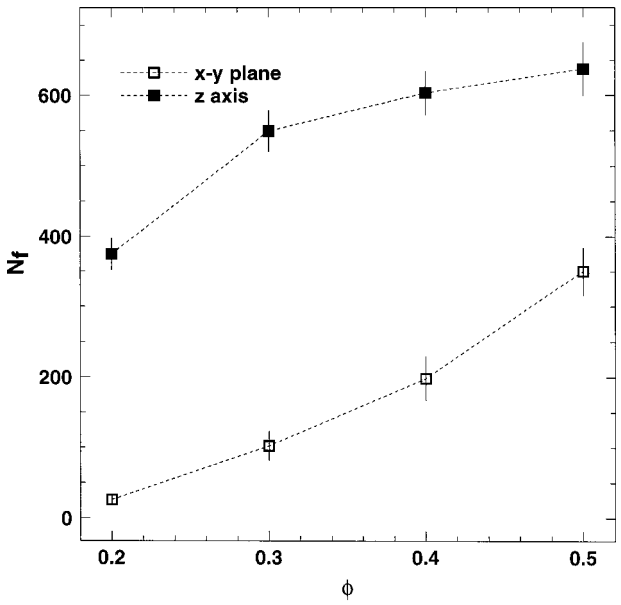

FIG. 19. The computed number of blows to failure is considerably greater along the z axis and is in fact nearly proportional to the fuse current, since the number of blows roughly counts the number of current paths.

thermal coefficient of resistivity, and this has been shown to be associated with the melting of crystalline polymer domains, with an associated large increase in the specific volume of the polymer.[8] Isothermal measurements on this material, with small, resistivity-measuring fields, clearly show a many-decade increase in the resistivity at the temperature at which the poly(ethylene) melts. These same materials are used as surge protectors, which work by being placed in series with a circuit, and therefore in normal operating mode

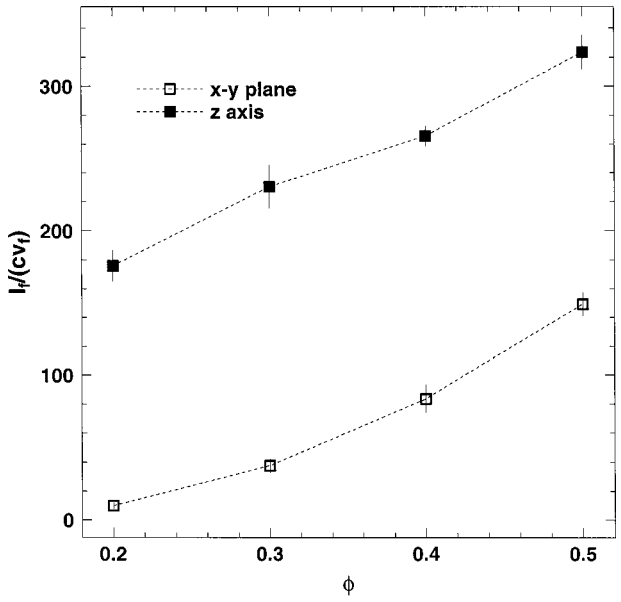

FIG. 20. The computed current required to fuse the macroscopic network as a function of particle volume fraction. Along the z axis the fuse current is considerably larger, as would be the fracture stress in a mechanical system. The fuse current is closely approximated by the conductivity, because the maximum fuse current occurs after just a few blows.

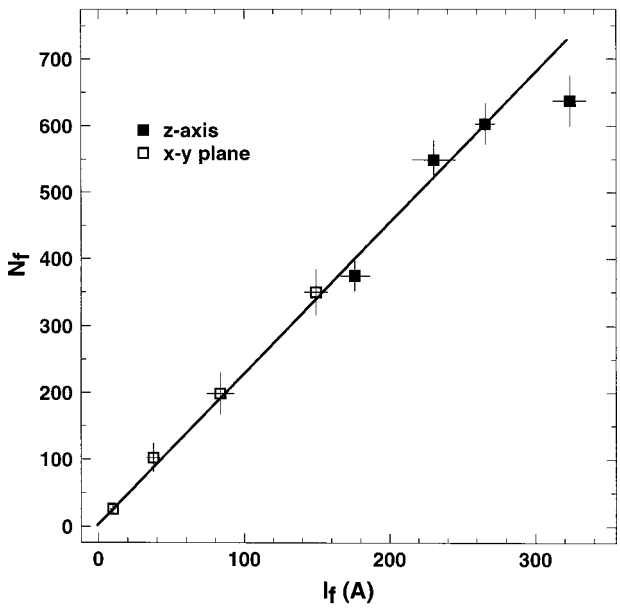

FIG. 21. The computed number of fuse blows is shown to be proportional to the fuse current. These data are for all particle concentrations and along both the x-y plane and the z axis.

have a much lower impedance than the circuit. When a voltage spike arrives at the surge protector, the surge protector heats up, driving up the resistivity sufficiently that the surge protector drops the voltage, thus sparing the circuit.

It is not yet understood exactly what the mechanism of this ''soft fusing'' is, but there are at least two basic scenarios, adiabatic and isothermal. As current is transported through the material, heat is generated at the particle contacts. If this local heating causes a hot contact to blow on time scales short compared to a characteristic thermal diffusion time, roughly the time it takes heat to diffuse the mean interparticle spacing, then the situation is adiabatic and, therefore, analogous to the simple conductor-insulator fuse model described above. If the system thermally equilibrates on time scales fast compared to contact blow times, then the system is isothermal, and the fuse model we have presented may have no bearing on this problem. If the applied voltage is low, then the system would tend to be isothermal: if the applied voltage is high, then the system would tend to be adiabatic.

We have investigated soft adiabatic fusing models where the contact conductance is described by $c=c_0/(1+i\Delta v/b)^{\alpha}$, in terms of the voltage drop Δv across the conductor and the current i passing through it. When the exponent $\alpha=1$, the network does not show any instabilities, and the network resistance changes continuously and slowly with applied voltage. When $\alpha=2$, the network is unstable, with platelike instabilities containing low-conductance conductors, and the resistance changes much more rapidly with applied voltage, much as in the conductor-insulator fuse model. An approach such as this might be appropriate to these materials, when used as surge protectors.

V. CONCLUSIONS

We have investigated the dielectric breakdown strength of electric-field-structured materials having $BaTiO_3$ as the par-

ticulate phase and amine-cured EPON 828 as the resin. Our experimental results indicate roughly a 50% enhancement in the dielectric breakdown strength in the x-y plane over that of the z axis, which is slightly below that of the unstructured control sample. These results can be rationalized in terms of a voltage-driven resistor-short breakdown model that we applied to simulated field-structured composites. This model demonstrates a substantial increase in the breakdown strength in the x-y plane over the z axis, in good agreement with our data, and also shows that this enhancement in dielectric breakdown strength should hold at high particle loadings, such as those used to encapsulate devices with high voltage power supplies.

Finally, we presented an investigation of a closely related network model, the conductor-insulator fuse model, in which the network fuses as the applied current increases. We show that this model is analogous to mechanical failure in spring networks, and we suggest that this model, and modifications thereof, might be relevant to carbon black/poly(ethylene) composites, when used as surge protectors.

ACKNOWLEDGMENTS

Sandia is a multiprogram laboratory operated by Sandia Corporation, a Lockheed Martin Company, for the U.S. Department of Energy under Contract No. DE-AC04-94AL8500. This work was supported by the Division of Materials Sciences, Office of Basic Energy Sciences, U.S. Department of Energy (DOE).

[1] J. E. Martin, R. A. Anderson, and C. P. Tigges, in *Nanostructured Materials: Clusters, Composites, and Thin Films*, edited by V. M. Shalaev and M. Moskovits, ACS Symposium Series No. 679 (American Chemical Society, Washington, D.C., 1998), pp. 54–69.

[2] J. E. Martin, R. A. Anderson, and C. P. Tigges, J. Chem. Phys. **108**, 3765 (1998).

[3] T. C. Halsey, R. A. Anderson, and J. E. Martin, in *Proceedings of the 5th International Conference on Electro-rheological Fluids, Magneto-rheological Suspensions and Associated Technology*, edited by W. A. Bullough (World Scientific, Singapore, 1996), p. 192.

[4] T. C. Halsey, R. A. Anderson, and J. E. Martin, Int. J. Mod. Phys. B **10**, 3019 (1996).

[5] J. E. Martin, R. A. Anderson, and C. P. Tigges, J. Chem. Phys. **108**, 7887 (1998).

[6] L. A. Dissado and P. J. J. Sweeney, Phys. Rev. B **48**, 16 261 (1993).

[7] B. Last and D. Thouless, Phys. Rev. Lett. **27**, 1719 (1971).

[8] M. B. Heaney, Appl. Phys. Lett. **69**, 2602 (1996).